Preliminary results of iterative 1D imaging with the hybrid penalty function

Mandy Wong and Antoine Guitton

ABSTRACT

The hybrid penalty function (HPF) varies from ℓ^1 to ℓ^2 smoothly, thus offering opportunities for (1) robust optimization when non-Gaussian noise is present in the data and (2) sparseness regularization when blocky or spiky models are needed. Using a solver designed to minimize the HPF and a 1D migration operator, both properties are tested and inversion results compared with those obtained with the ℓ^2 norm. The HPF yields sparse, noise free reflectivity series. The choice of parameters controlling the sparseness behavior remains difficult. More realistic 2D and 3D examples should follow.

INTRODUCTION

In seismic imaging, reflectivity models in the subsurface are often made up of a series of sharp and sparse signals. As an adjoint operation to the forward modeling operator, migration alone might not be adequate to recover the correct reflectivity series of the subsurface. As a results, least-squares migration (LSM) (Lambare et al., 1992; Nemeth et al., 1999) or iterative imaging with the ℓ^2 norm was developed to strive for a better solution. Many studies have shown that a least-squares migration image has fewer migration artifacts, better relative amplitude information, and higher resolution than the corresponding migration image (Clapp, 2005; Valenciano, 2008; Wong et al., 2012). However, when the data are contaminated with non-Gaussian noise (e.g, noise bursts, spikes), least-squares migration might not be an ideal solution for inversion as the penalty function over-emphasizes large values in the residual. In addition, if sparseness is expected in the migrated image to highlight regions of strong impedance contrast, a regularization term with a ℓ^1 norm behavior needs to be added to the data fitting part. In both cases, the hybrid penalty function (HPF) with the correct parameterization for measuring data and model misfit is more appropriate because it varies smoothly between the ℓ^2 norm for small residuals and ℓ^1 norm for high residuals. Being convex, a fast solver based on a non-linear conjugate direction method can be used to minimize the HPF efficiently (Claerbout, 2014b).

We apply iterative imaging on two 1D synthetic examples using a HPF and ℓ^2 solver. The first case has clean, noise-free data and the second case has random noise-bursts in the data. The inversion results between the two cases with the two solvers show that using the hybrid penalty function provides the best solution. These

results rely heavily on our ability to select a judicious set of parameters controlling the ℓ^2/ℓ^1 behavior of the HPF, as well as the strength of the regularization term. Our goal is to apply the HPF on bigger datasets in 2D and 3D.

In this paper, we begin by introducing the HPF and the objective function we are minimizing, along with the modeling/migration operators. Then we show on a simple 1D example how the iterative imaging performs when non-Gaussian noise is present in the data and sparse reflectivities are sought.

THEORY

We now present the hybrid penalty function and its main properties, as well as the modeling/migration operators.

Hybrid Penalty Function

The Hybrid Penalty Function (HPF) (Claerbout, 2014b) is a convex penalty function that varies smoothly from ℓ^2 to ℓ^1. Equation (1) below presents the HPF function, $H(r)$, and its derivatives:

$$\begin{aligned} H(r) &= \sqrt{1+(gr)^2}-1, \\ H'(r) &= gr/\sqrt{1+(gr)^2}, \\ H"(r) &= 1/(1+(gr)^2)^{3/2}, \end{aligned} \tag{1}$$

where g is a constant that scales the residual r. The first derivative, $H'(r)$, behaves like the first derivative of the ℓ^2 norm at small $|gr|$. At large $|gr|$, it behaves as the first derivative of the ℓ^1 norm. In practice, the factor g is often taken to be the inverse of the value of some percentile of residual magnitudes. Its value determines what part of the residual is treated as ℓ^1 and what part is treated as ℓ^2. The HPF is minimized with a non-linear conjugate direction solver and is described in Claerbout (2014b), Chapter 6.

In the iterative imaging problem, we expect the reflectivity model to be made up of a series of sharp and sparse signals. We include a model-styling goal to promote sparseness of the solution. The desired objective function $S(\mathbf{m})$ becomes:

$$S(\mathbf{m}) = H_d(\mathbf{Lm}-\mathbf{d}) + \epsilon H_m(\mathbf{m}), \tag{2}$$

where $\mathbf{L}$ represents the Born modeling operator acting onto the reflectivity model $\mathbf{m}$, and $\mathbf{d}$ is the observed data. H_d and H_m are HPF for the data-fitting and model-styling goal, respectively. Three constants need to be chosen in equation (2): two thresholds values g_d and g_m that regulate the transitioning behavior between ℓ^2 and ℓ^1 in the hybrid penalty function, and ϵ that tunes the relative strength of the regularization with respect to the data-fitting goal. We selected g_d to make sure that the spikes in the data would be treated with ℓ^1 and signal with ℓ^2. For a synthetic dataset, this

can be easily done. On the contrary, ϵ and g_m were selected by trial and error, which is not a robust way when expensive operators and large datasets are used. To address this issue, Claerbout (2014a) proposes an automatic way of finding the thresholds of the HPF using the Jensen inequality. At this stage, we have yet to test this scheme.

Migration and modeling operators

The Born modeling operator is constructed by linearizing the full-wave equation with respect to the reflectivity model. The linear relationship between synthetic data, $d(x_r, \omega)$, and model, $m(y)$, is:

$$\begin{aligned} d(x_r, \omega) &= -\int G_o(x_r, \omega; y) m(y) \omega^2 G_o(y, \omega; x_s) f_s(\omega) dy, & (3) \\ &= \mathbf{Lm}, & (4) \end{aligned}$$

where $G_o(x, \omega; y)$ represents the Green's function of the acoustic wave equation, propagating energy from location y to x at frequency ω, and $f_s(\omega)$ is the source wavelet. Mathematically, the adjoint of the modeling operator is the cross-correlation imaging condition $\mathbf{m} = \mathbf{L}^*\mathbf{d}$:

$$\begin{aligned} m_{mig}(\mathbf{y}) &= \mathbf{L}^T\mathbf{d}, & (5) \\ &= -\int d\mathbf{x}_r \int d\mathbf{x}_s \int d\omega \left(\omega^2 G_o^*(\mathbf{y}, \omega; \mathbf{x}_s) f_s(\omega) G_o^*(\mathbf{x}_r, \omega; \mathbf{y}) d(\mathbf{x}_r, \omega)\right). & (6) \end{aligned}$$

In our study, we use the two-way acoustic wave-equation to generate the Green's functions.

SYNTHETIC EXAMPLES

We present results of iterative 1D imaging with two velocity models: a smooth velocity model emulating a sedimentary environment, and the same velocity model with a salt body added. These two models are used to generate 1D traces with Born modeling. The inversion of these traces with and without noise added, with and without regularization, are presented here.

Sediment velocity model

We construct a simple 1D model made of a linearly increasing velocity that resembles a sediment profile. A reflectivity model is created with a sharp positive pulse at z = 2000

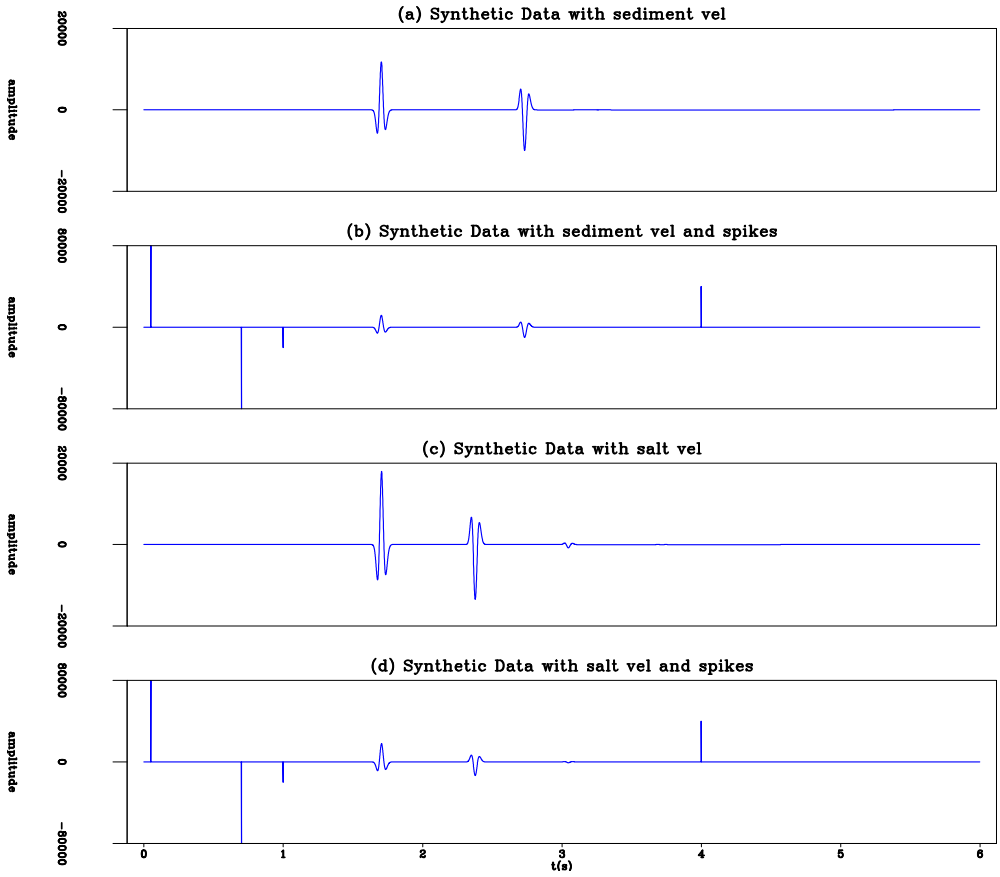

Figure 1: Input data for iterative inversion. (a) is synthetic data using sediment velocity and (b) shows the same dataset as (a) with added spikes. (c) is the synthetic dataset using a velocity with salt structure and (d) shows the same dataset as (c) with added spikes. Notice the relative strength of the spikes is much higher than the signal. [**ER**]

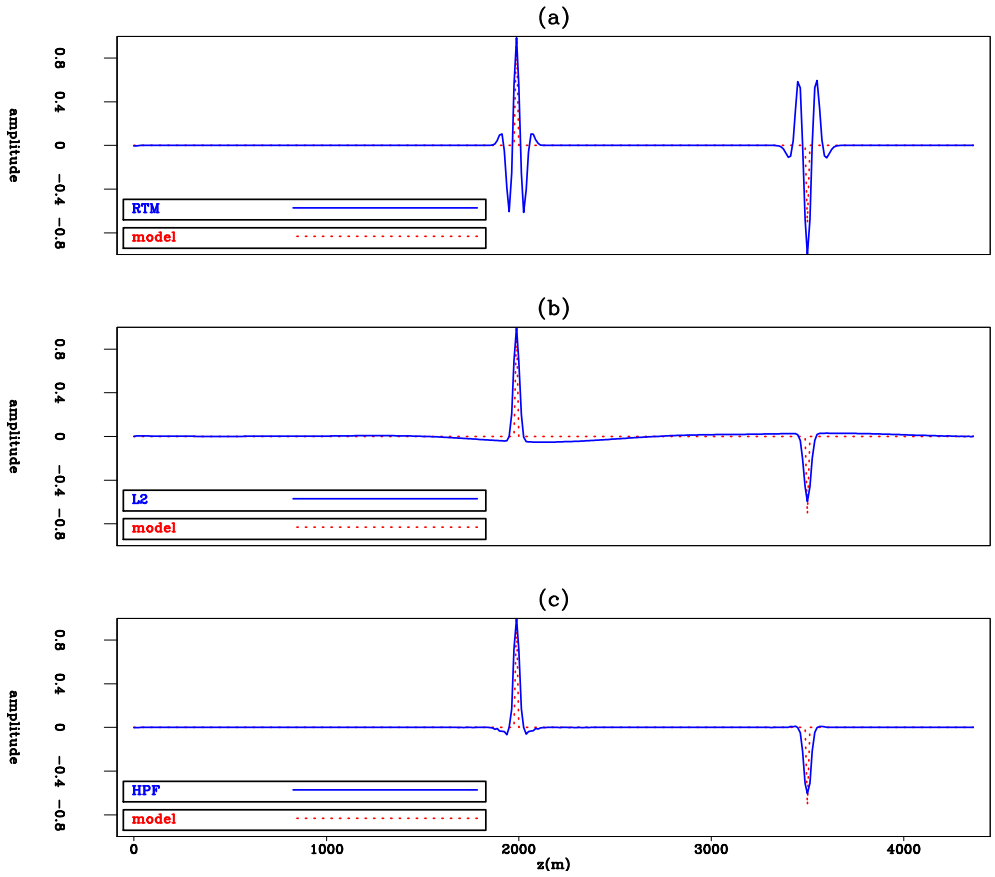

Figure 2: Recovered reflectivity model for the case of sediment velocity and clean data (Figure 1a). (a) reverse-time migration, (b) least-squares migration, and (c) iterative inversion with hybrid penalty function. [**ER**]

m and a negative pulse at z = 3500 m. Figure 1a shows the resulting synthetic data. All migrations and iterative imaging use the correct velocity model. In this simple 1D model, there is no geometrical spreading effect, wavelet stretching, or positioning error due to incorrect velocity. It is no surprise to see that even the reverse-time migration (RTM) (Figure 2a) image provide a fairly accurate representation of the input model. Figure 2b shows the iterative imaging result. It has a broader spectrum and better relative-amplitude information than the RTM image (Figure 2a). The results between the iterative imaging with HPF (Figure 2c) and with the ℓ^2 norm (Figure 2b) are very similar. However, the regularization term present in equation (2) helps by removing the low frequency component visible in the Figure 2b.

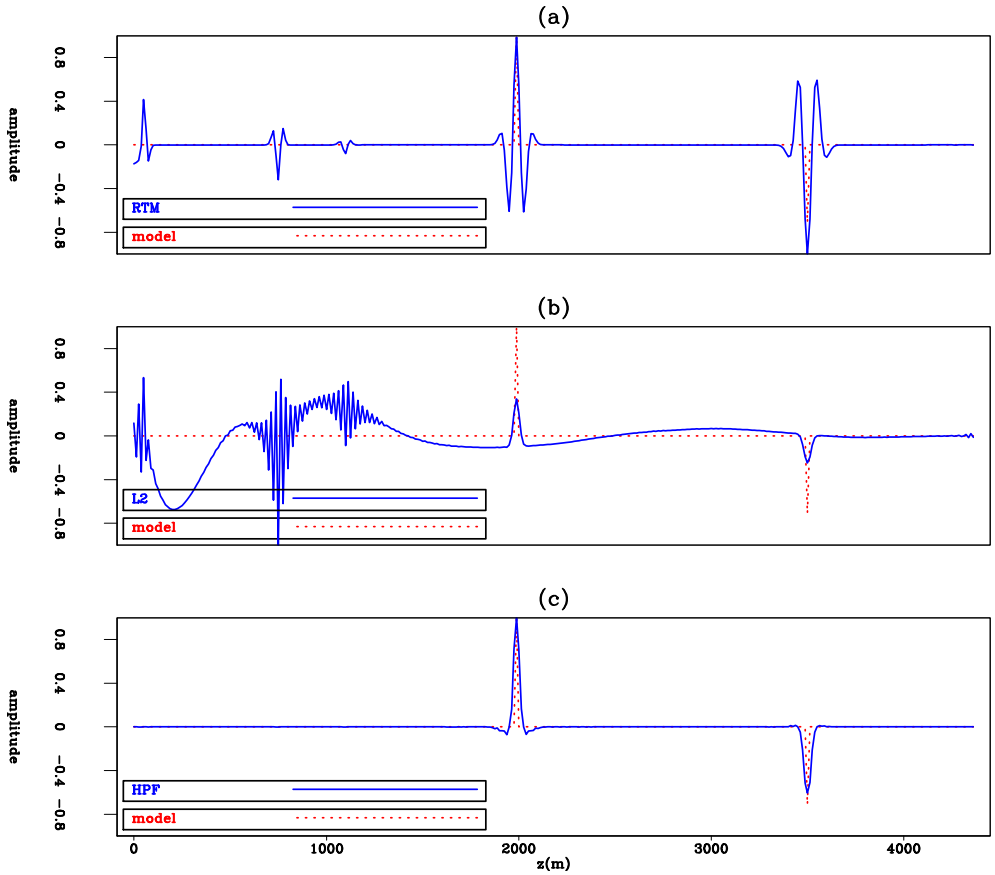

Figure 3: Recovered reflectivity model for the case of sediment velocity and spiky data (Figure 1b). (a) reverse-time migration, (b) least-squares migration, and (c) iterative inversion with hybrid penalty function. [**ER**]

Next, we add random noise-bursts to the synthetic data to account for the effects of non-Gaussian noise in the data. Figure 1b shows the resulting spiky data. Notice that the amplitude of some bursts is much higher than the amplitude of the signal. As a result of the added noise, the RTM image (Figure 3a) is now contaminated with several spurious reflectors. Applying LSM (Figure 3b) does not properly remove the artifacts. On the other hand, iterative imaging with HPF removes the spurious reflectors in the image and recovers a relatively accurate reflectivity model (Figure

3c).

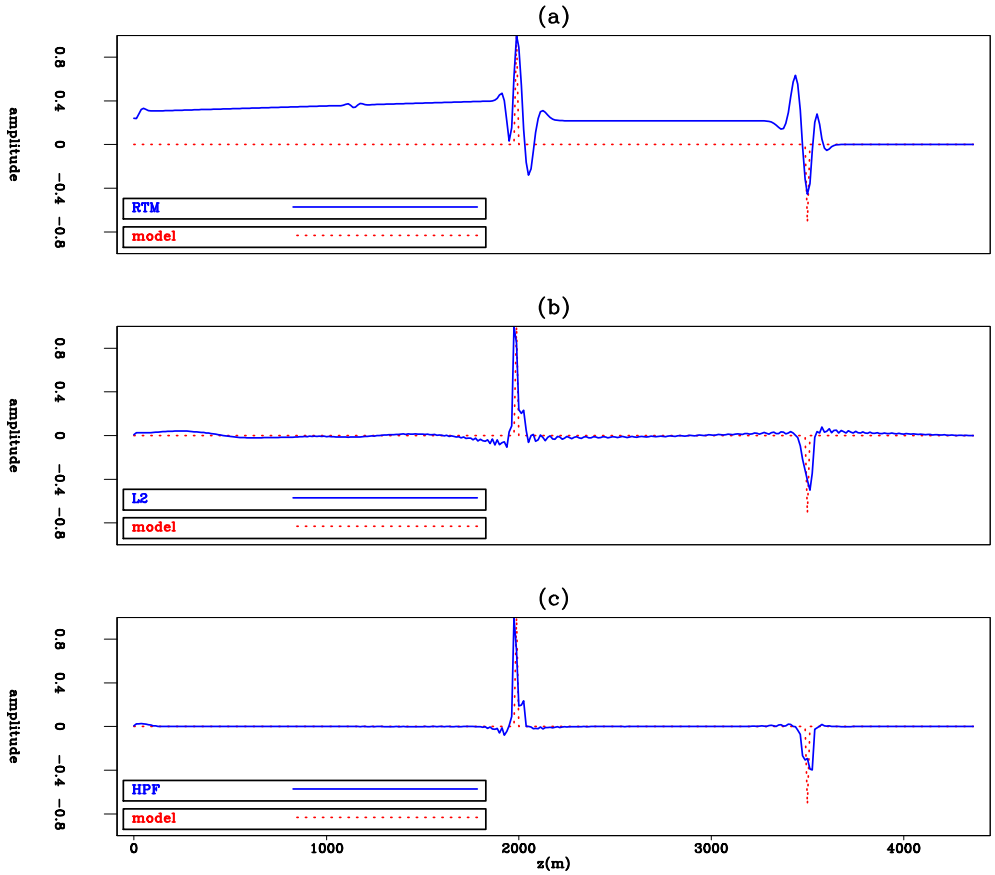

Figure 4: Recovered reflectivity model for the case of salt velocity and clean data (Figure 1c). (a) reverse-time migration, (b) least-squares migration, and (c) iterative inversion with hybrid penalty function. [**ER**]

Sediment velocity model with salt

We increase the level of complexity by adding a salt layer to the velocity model. The top and base of the salt layer coincide with the location of the reflectivity pulses. Figures 1c and 1d show the resulting synthetic data with and without random noise-bursts, respectively. The RTM image (Figure 4a) now contains the traditional high-amplitude low-frequency RTM artifacts above the salt layer. There is also a small crosstalk artifact near z = 1200 m. Figures 4b and 4c show the iterative 1D imaging result using the ℓ^2 norm and the HPF, respectively. Iterative imaging can successfully remove the above-mentioned artifacts using either cost function. However, the reflectivity recovery is not perfect because of wavelet stretching in the region with high velocity. When the data are contaminated with random noise-bursts, iterative imaging with the ℓ^2 norm (Figure 5b) is unable to remove the noise artifacts in the image. Iterative imaging with HPF gives a much more satisfactory solution (Figure

5c).

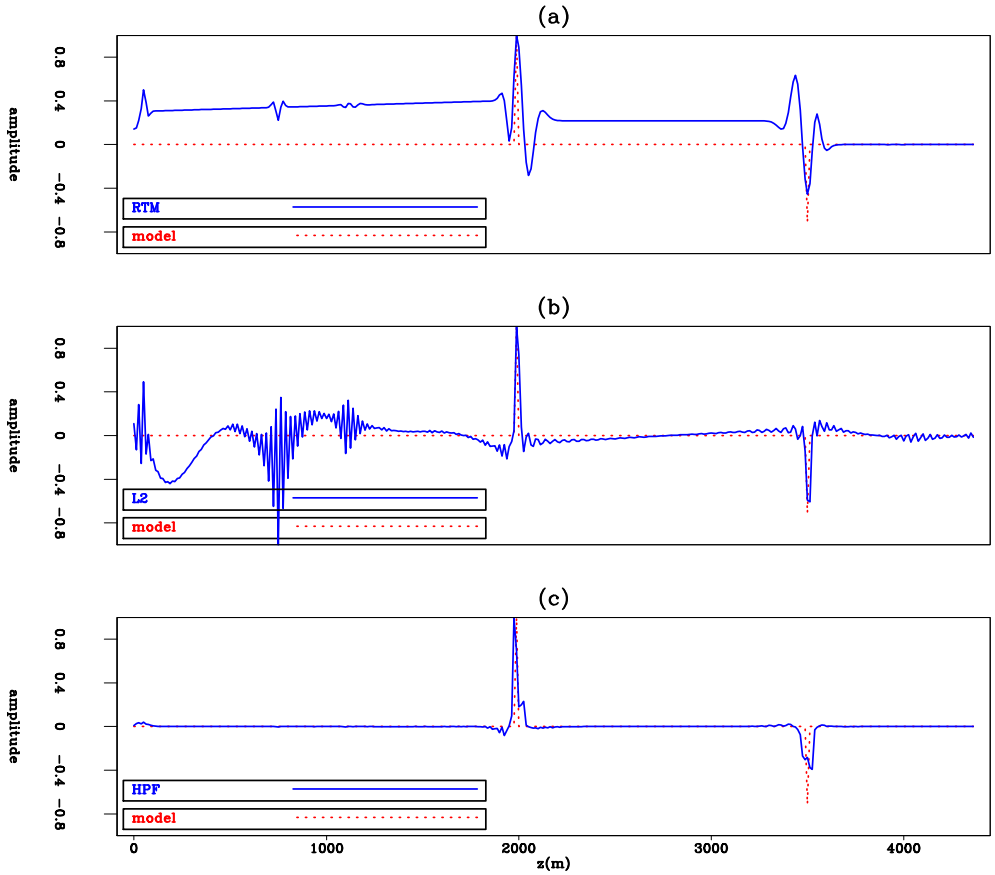

Figure 5: Recovered rflectivity model for the case of salt velocity and spiky data (Figure 1d). (a) reverse-time migration, (b) least-squares migration, and (c) iterative inversion with hybrid penalty function. [**ER**]

CONCLUSION

We compare inversion results of iterative 1D imaging using the ℓ^2 norm and the hybrid penalty function based on several 1D models. When random noise-bursts are added to the data, least-squares migration fails to remove migration artifacts. On the contrary, because it varies from ℓ^2 to ℓ^1, the hybrid penalty function helps recover a sparse and noise-free reflectivity series. Our results are, at this stage, preliminary. More work needs to be done to (1) select the right parameters for the inversion and (2) invert more realistic datasets in 2D and 3D.

ACKNOWLEDGMENTS

Antoine Guitton acknowledges GeoImaging Solutions Inc. for financial support.

REFERENCES

Claerbout, J., 2014a, Automatic default for hyperbolic softclip: SEP Report, **152**.

Claerbout, J. F., 2014b, Geophysical image estimation by examples.

Clapp, M. L., 2005, Imaging under salt: illumination compensation by regularized inversion: PhD thesis, Stanford University.

Lambare, G., J. Virieux, R. Madariaga, and S. Jin, 1992, Iterative asymptotic inversion in the acoustic approximation: Geophysics, **57**, 1138–1154.

Nemeth, T., C. Wu, and G. T. Schuster, 1999, Least-squares migration of incomplete reflection data: Geophysics, **64**, 208–221.

Valenciano, A., 2008, Imaging by Wave-Equation Inversion: PhD thesis, Stanford University.

Wong, M., B. Biondi, and S. Ronen, 2012, Imaging with multiples using linearized full-wave inversion: SEG Expanded Abstracts, 1–5.